PHYSICS

Zero–trade-off multiparameter quantum estimation via simultaneously saturating multiple Heisenberg uncertainty relations

Zhibo Hou[1,2]*, Jun-Feng Tang[1,2]*, Hongzhen Chen[3], Haidong Yuan[3†], Guo-Yong Xiang[1,2†], Chuan-Feng Li[1,2], Guang-Can Guo[1,2]

Quantum estimation of a single parameter has been studied extensively. Practical applications, however, typically involve multiple parameters, for which the ultimate precision is much less understood. Here, by relating the precision limit directly to the Heisenberg uncertainty relation, we show that to achieve the highest precisions for multiple parameters at the same time requires the saturation of multiple Heisenberg uncertainty relations simultaneously. Guided by this insight, we experimentally demonstrate an optimally controlled multipass scheme, which saturates three Heisenberg uncertainty relations simultaneously and achieves the highest precisions for the estimation of all three parameters in SU(2) operators. With eight controls, we achieve a 13.27-dB improvement in terms of the variance (6.63 dB for the SD) over the classical scheme with the same loss. As an experiment demonstrating the simultaneous achievement of the ultimate precisions for multiple parameters, our work marks an important step in multiparameter quantum metrology with wide implications.

INTRODUCTION

High-precision measurement and estimation is one of the main driving forces for science and technology. Quantum metrology, which uses quantum mechanical effects such as superposition and entanglement, promises higher precisions than the classical scheme. A widely used tool that characterizes the ultimate precision in quantum metrology is the quantum Cramér-Rao bound, a generalization of the Cramér-Rao bound in the classical estimation (*1*–*11*). The symmetric logarithm operator (SLD, denoted as L_x), which is the solution to the equation $\frac{\partial \rho_x}{\partial x} = \frac{1}{2}(L_x\rho_x + \rho_x L_x)$ with x as the unknown parameter, plays a particular important role in the quantum Cramér-Rao bound. Not only can the SLD be used to obtain the quantum Fisher information as $F = \mathrm{Tr}(\rho_x L_x^2)$, which is a central quantity in the quantum Cramér-Rao bound, but the SLD can also be used to identify the optimal measurement as the projective measurement on the eigen-spaces of the SLD (*1*).

Such characterization of the precision, however, lacks a direct physical picture. A more fundamental tool related to the ultimate precision is the Heisenberg uncertainty relation (*3*, *12*), which is also more physical. The role of the uncertainty relation in quantum metrology, however, has only been investigated in the single-parameter quantum estimation (*3*). For multiparameter quantum estimation (*13*–*31*), multiple uncertainty relations are involved. The interplay among multiple uncertainty relations, however, remains a largely unexplored territory. One motivation of this study is to characterize the precisions of multiple parameters from the uncertainty principle, which can, in turn, shed light on the study of the uncertainty relations and cross-fertilize both fields. The central motivation of this study, however, is experimental. While the theory of quantum metrology has been developed toward more complex scenarios involving multiple parameters (*13*–*25*), the experimental studies are still largely on the estimation of a single parameter (*6*–*10*, *32*). There are only a few experiments on multiparameter estimation (*26*–*31*, *33*–*36*), and these previous experiments cannot achieve the highest precisions for all parameters simultaneously. The improvements are always hampered by the trade-offs induced by the incompatibility of the optimal protocols for the estimation of different parameters. Our study provides the first experimental demonstration of an optimally controlled multiparameter quantum estimation that achieves the highest precisions for all parameters simultaneously.

RESULTS

Connecting quantum metrology with Heisenberg uncertainty relations

We study multiple Heisenberg uncertainty relations with the estimation of the three parameters for operators in the special unitary group SU(2). This is a fundamental problem in quantum metrology as it arises frequently in many practical applications, such as quantum gyroscope, quantum reference frame alignments, and quantum sensing (*37*, *38*). The protocol has only been theoretically investigated using the quantum Fisher information matrix and the quantum Cramér-Rao bound (*19*), the statistical tools generalized from classical statistics.

A general operator in SU(2) can be written as $U_s = e^{-i\alpha\vec{n}\cdot\vec{\sigma}}$, with $n = (\sin\theta\cos\phi, \sin\theta\sin\phi, \cos\theta)$ and $\sigma = (\sigma_1,\sigma_2,\sigma_3)$ as the Pauli operators. The three parameters that characterize the operator are $\alpha \in [0, \pi/2]$, $\theta \in [0, \pi]$ and $\phi \in [0, 2\pi)$, which are the parameters to be estimated in our dynamically controlled scheme as shown in Fig. 1A. For each parameter, the Heisenberg uncertainty relation, independent of the quantum Cramér-Rao bound, puts a fundamental limit on the achievable precision as (see Materials and Methods)

$$\delta\hat{x}^2\langle\Delta H_x^2\rangle \geq \frac{1}{4} \quad (1)$$

[1]CAS Key Laboratory of Quantum Information, University of Science and Technology of China, Hefei 230026, P. R. China. [2]CAS Center For Excellence in Quantum Information and Quantum Physics, University of Science and Technology of China, Hefei 230026, P. R. China. [3]Department of Mechanical and Automation Engineering, The Chinese University of Hong Kong, Shatin, Hong Kong.
*These authors contributed equally to this work.
†Corresponding author. Email: hdyuan@mae.cuhk.edu.hk (H.Y.); gyxiang@ustc.edu.cn (G.-Y.X.)

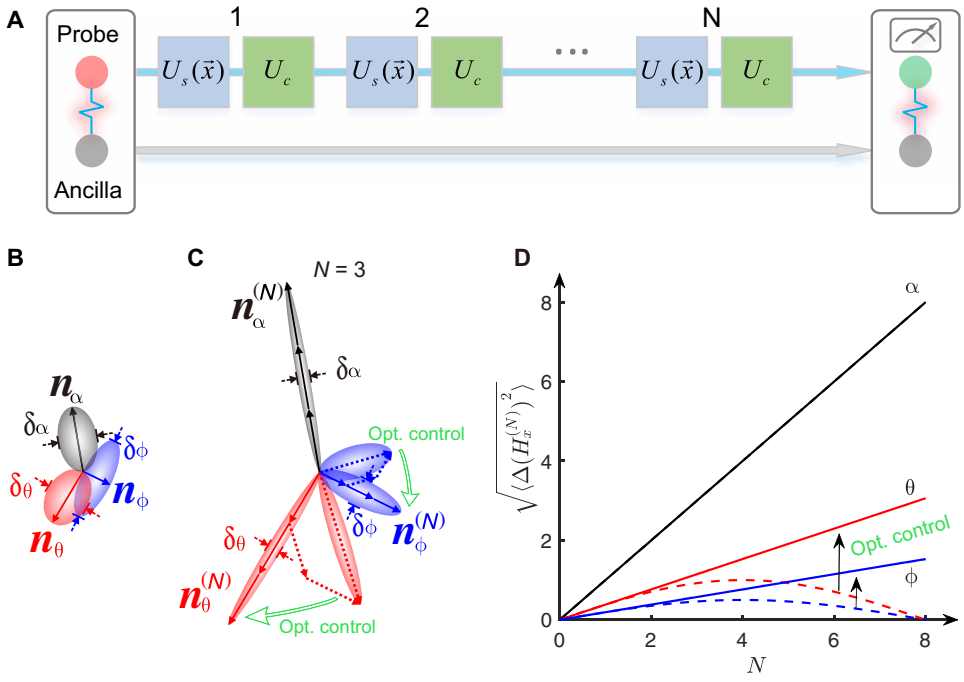

Fig. 1. Control-enhanced sequential simultaneous measurement. (**A**) Sequential scheme with controls. The system qubit is maximally entangled with an ancilla and operated by N copies of a multiparameter channel sequentially, with controls inserted in between. Projective measurements on the Bell basis are performed on the system-ancilla to measure all parameters simultaneously. (**B**) Generators of one operator U_s. The Bloch vectors of the three generators, n_x with $x \in \{\alpha, \theta, \phi\}$, are plotted, where the length represents its maximal SD. The width in the other direction of the ellipsoid is the minimum SD for the estimation of the parameter. (**C**) Generators with N copies of operators [$N = 3$ in (C)]. Without the controls, the length of the generators do not always increase linearly with N due to the noncommutativity. With the optimally designed controls, the length of all three generators increase linearly with N, which minimizes the SD of the estimations for all three parameters. (**D**) SDs of the three generators with respect to N. While the SD of the generator for α increases linearly with N even without control, the SD of the generators for θ and ϕ increases linearly with N only with the optimally designed control.

where $x \in \{\alpha, \theta, \phi\}$, $\delta\hat{x}^2$ is the variance of the estimator, and $\langle \Delta H_x^2 \rangle = \langle \Psi_x | H_x^2 | \Psi_x \rangle - \langle \Psi_x | H_x | \Psi_x \rangle^2$ is the variance of H_x with $H_x \equiv i(\partial_x U_s) U_s^\dagger$ as the corresponding generator of the parameter (*5*, *39*, *40*).

To achieve the best precision for each parameter, one needs to maximize the variance of the corresponding generator. In the Supplementary Materials, we show that the variance of these generators are upper bounded as

$$\langle \Delta H_\alpha^2 \rangle \leq 1, \langle \Delta H_\theta^2 \rangle \leq \sin^2\alpha, \langle \Delta H_\phi^2 \rangle \leq \sin^2\alpha \sin^2\theta \quad (2)$$

These upper bounds can be saturated separately with the corresponding optimal probe states.

The condition for an observable, denoted as O_x, to achieve the minimal uncertainty in inequality 1 is

$$(H_x - \langle H_x \rangle) | \Psi_x \rangle = i\gamma (O_x - \langle O_x \rangle) | \Psi_x \rangle \quad (3)$$

where γ is an arbitrary real scalar (*41*). For each particular parameter, by performing the projective measurement on the eigenvectors of such observable, the minimum $\delta\hat{x}$ can be achieved (see Materials and Methods). Such measurement does not have to be the projective measurement on the eigen-spaces of $L_x = 2(|\partial_x \Psi_x\rangle\langle\Psi_x| + |\Psi_x\rangle\langle\partial_x \Psi_x|)$, a widely used SLD for pure state (see the Supplementary Materials).

If N copies of the operator can be used in each time, the architecture of arranging the N operators also needs to be optimized. Besides the control-enhanced sequential scheme in Fig. 1, the N operators can also be arranged in parallel, as shown in Fig. 2, where the probe states can be either separated or entangled. For all architectures with N copies of the operator, the variance of the generator $H_x^{(N)}$ is always upper bounded as (*42*)

$$\left\langle \Delta \left[H_x^{(N)} \right]^2 \right\rangle \leq N^2 \langle \Delta H_x^2 \rangle \quad (4)$$

which leads to the Heisenberg limit

$$\delta\hat{x}^2 \geq \frac{1}{4N^2 \langle \Delta H_x^2 \rangle} \quad (5)$$

When the procedure is repeated n times, this gives the ultimate lower bound on the minimal variance of the estimation, $\delta\hat{x}^2 \geq \frac{1}{4nN^2\langle \Delta H_x^2 \rangle}$. For a single parameter, this ultimate lower bound can always be saturated.

Simultaneous estimation of multiple parameters with incompatible generators

The generators for the three parameters, denoted as H_α, H_θ, and H_ϕ, do not commute with each other. This causes some doubts on the achievability of the ultimate precision for all three parameters simultaneously, just as the Heisenberg's uncertainty principle fundamentally constraints the joint measurement. However, the noncommuting generators do not prohibit the simultaneous optimal estimation of the three parameters. The minimal variances can be

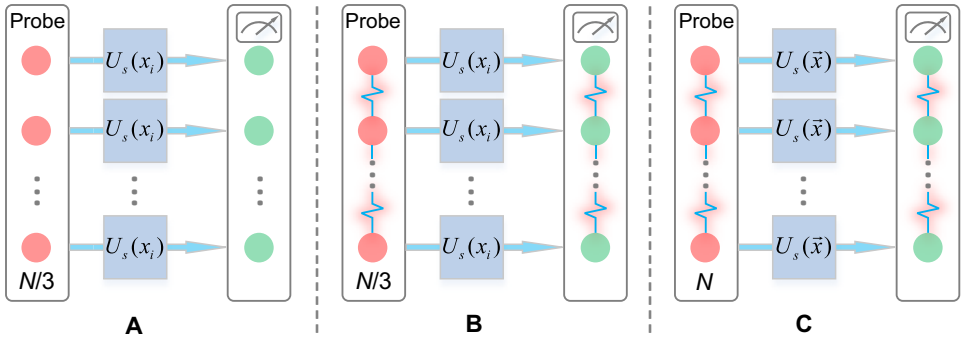

Fig. 2. Three other schemes. (**A**) Classical individual measurement. (**B**) Entangled individual measurement. (**C**) Entangled simultaneous measurement. In the two individual measurements, (A) and (B), the *N* copies of the operator are evenly divided into three groups, and one group is used to estimate one parameter. The difference between (A) and (B) is that (A) only uses separable states and separable measurements, while (B) allows entangled states and collective measurements in each group. The entangled simultaneous measurement in (C) does not divide the *N* operators into three groups but uses them together to estimate all three parameters simultaneously. The precision that can be achieved under these schemes are provided in the Supplementary Materials. None of them can achieve the best precision of all parameters simultaneously.

achieved simultaneously if the optimal probe states and the optimal architecture of arranging the *N* operators are the same, and the optimal measurements are compatible. These conditions are generally very difficult to satisfy. For example, under the parallel scheme as in Fig. 2C, where *N* qubits are prepared in a large entangled state with each qubit going through one operator, it is not possible to achieve the minimal variance for all three parameters simultaneously (*17*, *18*). However, these conditions can be satisfied under the optimally controlled sequential scheme.

Here, we experimentally implement the control-enhanced sequential scheme (*19*). In this scheme, the *N* operators, U_s, are arranged sequentially where additional controls, U_c, can be inserted (see Fig. 1A). Under such scheme, the total evolution is given by U_{cs}^N with $U_{cs} = U_c U_s$, and the generators of the parameters can be obtained as

$$H_x^{(N)} = i\left(\partial_x U_{cs}^N\right)\left(U_{cs}^N\right)^\dagger = \sum_{k=0}^{N-1} U_{cs}^k H_x \left(U_{cs}^k\right)^\dagger \quad (6)$$

where $x \in \{\alpha, \theta, \phi\}$. We note that the controls, which can be optimized to improve the precision, play an essential role to saturate the multiple uncertainty relations. Without the controls, the upper bound in inequality 4 is, in general, not achievable. For example, without the controls (which corresponds to setting $U_c = I$), the variance of the generator for θ cannot saturate the upper bound in inequality 4 since U_s do not commute with H_θ. This is illustrated in Fig. 1 (C and D). However, if additional controls are available, one can use proper controls to make U_{cs} commute with H_x, then from Eq. 6, it is easy to see that $H_x^{(N)} = NH_x$, the bound in inequality 4 is then saturated. To simultaneously achieve the minimal variance of all three parameters, the same control needs to work for all three parameters, i.e., the control should make U_{cs} commute with all three generators H_α, H_θ, and H_ϕ simultaneously. Such control actually exists. Specifically, we can choose $U_c = U_s^\dagger$, in this case $U_{cs} = I$, which commutes with all generators. However, as the parameters are not known a priori, this control can only be implemented adaptively as $U_s^\dagger(\hat{\alpha}, \hat{\theta}, \hat{\phi})$ with $\hat{\alpha}, \hat{\theta}, \hat{\phi}$ as the estimators obtained from previous data. In the asymptotical limit, the upper bound in inequality 4 can be saturated simultaneously for all three parameters with noncommuting generators. In addition, with an ancillary qubit, the optimal probe state for each parameter can all be taken as the maximally entangled state, and the optimal O_x satisfying Eq. 3 for different parameters is compatible (see the Supplementary Materials). The ultimate precision of all three parameters can thus be achieved simultaneously without any trade-off.

Experimental results

We design an experiment to achieve the highest precision simultaneously for all three parameters of SU(2) operators. The experimental setup, as shown in Fig. 3, consists of three modules: preparing the optimal probe state, implementing the optimal control, and performing the optimal measurement (see Materials and Methods for experimental details). The probe state is first prepared as the maximally entangled state, $\frac{1}{\sqrt{2}}(|H, \text{up}\rangle + |V, \text{down}\rangle)$; here, one qubit is encoded in the polarization degree of the photon, which uses the horizontal (*H*) and vertical (*V*) polarization as the basis, and the other qubit is encoded in the path degree of the photon, which uses the up and down path as the basis. The polarization qubit then goes through the unknown operator, U_s, and the control, U_c, sequentially for *N* times (*7*, *10*, *32*), where the control is designed as $U_c = U_s^\dagger(\hat{\alpha}, \hat{\theta}, \hat{\phi})$ and updated adaptively with the accumulation of the measurement data. A projective measurement on the common eigenvectors of three commuting observables, $\sigma_3\sigma_2$, $\sigma_1\sigma_3$, and $\sigma_2\sigma_1$, which are optimal for the estimation of α, θ, and ϕ, respectively (see the Supplementary Materials), is then performed.

We implement two sets of experiments. In the first set of experiments, the parameters are assumed to be within a small neighborhood of known values, and the adaptive controls are designed with this prior information. A unitary operator is considered with $\alpha = \frac{\pi}{4}$ and $\theta = \phi = \frac{\pi}{6}$ (the Supplementary Materials contains the result of another unitary operator). As shown in Fig. 4, the precision achieved in the experiment (green dots) is almost the same as the theoretical optimal precision of the control-enhanced sequential scheme (bottom solid line) for all three parameters (the differences between the experimental results and the optimal theoretical precision are listed quantitatively in table S1). Compared to the classical scheme, as in Fig. 2A, the experimentally achieved precision of the control-enhanced scheme at $N = 8$ has a 13.8-dB improvement in terms of the variance (6.9-dB improvement in terms of the SD). Compared to the highest precision that can be achieved under the parallel scheme with entangled probe states, the control-enhanced scheme

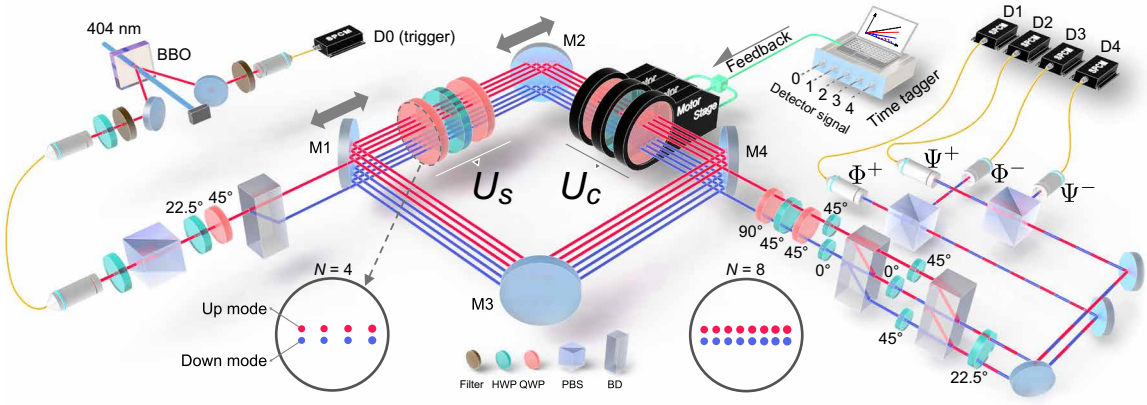

Fig. 3. Experimental setup. There are three modules in the experiment: state preparation, evolution, and measurement. The state preparation prepares probe-ancilla entangled state in the degree of polarization and path of a heralded single photon. In the evolution module, the probe qubit is operated by the unknown U_s and the adaptive control U_c for N times ($N = 4$ in the figure, and $N = 8$ is the largest in our experiment). In the measurement module, complete Bell measurements are performed on the probe and ancilla to extract information of U_s. Key components: polarization beam splitter (PBS), HWP, QWP, beam displacer (BD), and BBO.

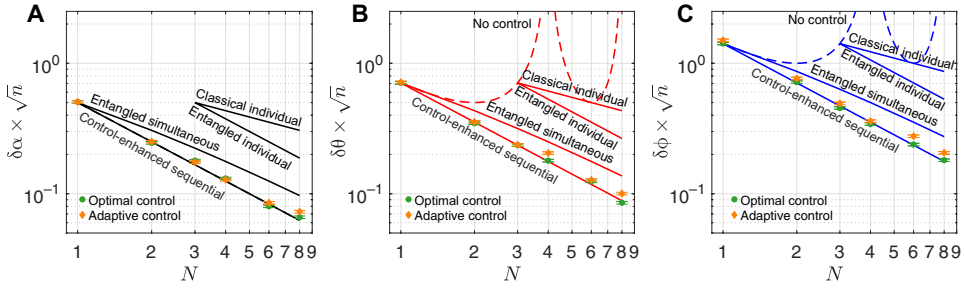

Fig. 4. Experimental results of the precision under the control-enhanced sequential scheme. (**A** to **C**) Experimental results for the three parameters in a U_s with $\alpha = \frac{\pi}{4}$ and $\theta = \phi = \frac{\pi}{6}$. The results are plotted together with the theoretical limit that can be achieved under the classical individual scheme (solid line named as "classical individual"), the entangled individual scheme (solid line named as "entangled individual"), and the entangled simultaneous estimation (solid line named as "entangled simultaneous") for comparison. The theoretical solid line (named as "control-enhanced sequential") of the control-enhanced sequential scheme for each parameter also represents the best precision that can be achieved in the single-parameter estimation. For the experiments with the optimal controls, each measurement is repeated $n = 1000$ times to get one estimation. The process is then repeated 1000 times to get 1000 estimations from which the SD of the estimation is obtained. For the experiments with the adaptive controls, each measurement is repeated 250 times during each step of the four adaptive procedures, an estimation is obtained after 1000 measurements (the estimation is obtained with all measurement results obtained during the four steps). The four-step adaptive process is then similarly repeated for 1000 times to get 1000 estimation, from which we obtain the SD of the estimation. The analysis of the error bars is given in Materials and Methods.

at $N = 8$ has a 3.8-dB improvement in terms of the variance (1.9-dB improvement in terms of the SD). For the given N, this is also the best one can hope to achieve for the simultaneous estimations of all three parameters, as the precision of each parameter has reached the ultimate limit. There are zero trade-offs among the precisions of different parameters.

The improvement above is based on the detected photons. If we take the loss into consideration, which includes the transmission efficiency, η_1 (in the experiment, $\eta_1 = 0.984$ for one loop), and the collection efficiency, η_2 (in the experiment, $\eta_2 = 0.48$), the improvement is 13.27 dB (in terms of the variance) compared with the classical scheme that uses the optical components of the same transmission and detection efficiency. The improvement is 10.05 dB if we compare with the lossless classical scheme (see the Supplementary Materials for the details).

In the second set of experiments, we do not assume the parameters are within small neighborhoods of known values. We adaptively update the controls after each 250 experiments and carry out 1000 experiments in each round. The controls are randomly chosen in the first 250 experiments and then updated on the basis of the measurement data. In each adaptive step, we use the maximum likelihood to update the estimation, which maximizes the posterior probability on the basis of all previous data. As shown in Fig. 4, the experiment results (diamonds) are close to the theoretical optimal values for all three parameters in the cases of $N = 1,2,3,4,6$, which indicates that the controls are already close to the optimal one after four steps of adaptation. In the case of $N = 8$, the SD of the experiment is slightly larger than the theoretical optimal value due to systematic errors but still outperforms the theoretical best value of the parallel scheme with the optimal entangled probe state (approximately 1.2-dB improvement in experiment, which is about 12.4 dB compared to the shot noise limit).

We also experimentally test the robustness of the scheme when the estimated value of the parameters, which are used to design the controls, is away from the true value. The robustness is tested against the deviation of each parameter, respectively. When N increases, the measurement scheme becomes more sensitive as expected, and its robustness against imperfect controls also decreases. Here, we show the experimental robustness of the most vulnerable case at $N = 8$ in Fig. 5. When there are deviations between the true

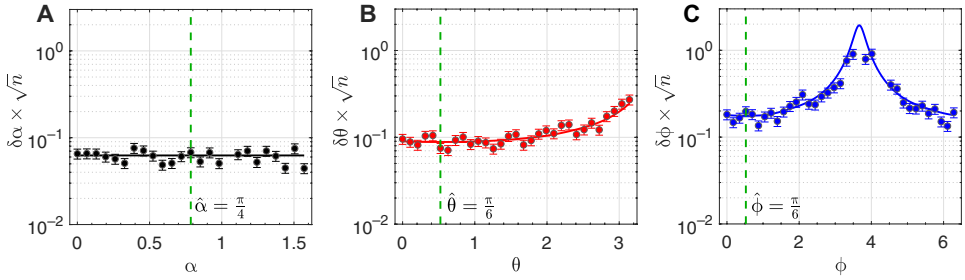

Fig. 5. Robustness of the experimental scheme with imperfect controls for *N* = 8. (**A** to **C**) Robustness for three parameters α, θ, and ϕ. The eight controls are designed according to $\hat{\alpha} = \frac{\pi}{4}$, $\hat{\theta} = \frac{\pi}{6}$, and $\hat{\phi} = \frac{\pi}{6}$, indicated by the green lines. The true values of α changes from 0 to $\frac{1}{2}\pi$, θ changes from 0 to π, and ϕ changes from 0 to 2π. Measurements for each dot are repeated with n = 1000 times to give an estimate, and this process is repeated 30 times to measure the SD of the estimate. The plotted error bars are analyzed in Materials and Methods.

values of α, θ, and ϕ and the values used in the control, the uncertainties of all three parameters are still close to their minimum (the intersection with the vertical dotted line, where the true value is equal to the value used in the control, which are taken as $\hat{\alpha} = \frac{\pi}{4}$, $\hat{\theta} = \frac{\pi}{6}$, and $\hat{\phi} = \frac{\pi}{6}$). Even at N = 8, the experimental results show a high level of robustness against the imperfections in the controls caused by the deviation between the estimated value and the true value. This robustness is inherent for the optimal control, as at the optimal point, the first-order derivative, which quantifies the effect of the deviation, is zero.

DISCUSSION

We showed that the zero–trade-off multiparameter quantum estimation is fundamentally equivalent to the saturation of multiple Heisenberg uncertainty relations simultaneously, which can be achieved if the same optimal probe state, the same optimal control, and commuting optimal observables can be identified. Guided by these conditions, we experimentally realized a scalable optimally controlled sequential scheme, which, for the first time, achieves the highest precisions with zero trade-off for the estimation of all three parameters in SU(2) operators. This opens the door for the exploration of multiple uncertainty relations in quantum metrology, which is also expected to play an important role in various other fields. We note that in our experiment, the control-enhanced scheme is demonstrated with single photons, which, however, is not a prerequisite. The scheme can also be implemented with more bright laser sources (*43*) as the photons are not required to be entangled with each other in the control-enhanced sequential scheme. This is different from the entangled parallel scheme where the brightness of the source decays quickly with the number of entangled photons, which limits the entangled parallel scheme to applications with delicate samples (*33*, *44*–*46*) that are sensitive to deleterious thermal effects (*47*).

MATERIALS AND METHODS

Parameter-based uncertainty relation from the general Heisenberg uncertainty principle

The precision limit is fundamentally related to the Heisenberg uncertainty principle (*3*, *40*). As given an observable O_x on the state $|\Psi_x\rangle$, the variance of the estimation is

$$\delta\hat{x} = \frac{\Delta O_x}{\left|\frac{\partial\langle O_x\rangle}{\partial x}\right|}$$

where $\Delta O_x = \sqrt{\langle \Delta O_x^2\rangle}$, $\langle O_x\rangle = \langle\Psi_x|O_x|\Psi_x\rangle$, and it is easy to get

$$\frac{\partial\langle O_x\rangle}{\partial x} = i\langle\Psi_x|[H_x, O_x]|\Psi_x\rangle$$

From the Heisenberg uncertainty relation,

$$\langle\Delta O_x^2\rangle\langle\Delta H_x^2\rangle \geq \frac{1}{4}\langle[H_x, O_x]\rangle^2 \quad (7)$$

we can immediately get $\delta\hat{x}^2\langle\Delta H_x^2\rangle \geq \frac{1}{4}$. It needs to be emphasized that this parameter-based uncertainty relation for characterizing estimation precision is completely derived using Heisenberg's uncertainty principle without using any results from statistical inference, which is not only more fundamental but also more accessible to the general physics community. The optimal observable that achieves the minimal uncertainty in Eq. 7 should satisfy $(H_x - \langle H_x\rangle)|\Psi_x\rangle = i\gamma(O_x - \langle O_x\rangle)|\Psi_x\rangle$.

Probe state preparation

To prepare the probe state, 1-mm-long β-barium borate (BBO) crystal, cut for type I phase–matched spontaneous parametric down-conversion (SPDC) process, is pumped by a 40-mW H-polarized continuous wave beam at 404 nm to generate a heralded single photon at the rate of 6000 per second (*48*), and then, a combination of half-wave plate (HWP) and quarter-wave plate (QWP) steers the photon to the state $\frac{1}{\sqrt{2}}(|H\rangle + |V\rangle)$. After passing through the beam displacer, the probe in the polarization degree of the photon is maximally entangled with the path degree of the photon as $\frac{1}{\sqrt{2}}(|H, \mathrm{up}\rangle + |V, \mathrm{down}\rangle)$.

Realization of the *N* controls

In the module of the evolution, as shown in Fig. 3, the operator U_s is implemented by a combination of two QWPs and an HWP, which is capable of generating arbitrary unitary operation on the polarization qubit. The control is realized by another set of two QWPs and an HWP, which are installed on three electric-motorized stages and can be rotated by feedback signals. Multiple passes of the qubit are realized by a cavity loop made of four mirrors. By carefully controlling the position of one mirror, we can control the number of passes (N) from 1 to 8 deterministically. For N = 8, there are eight beams in the up and down plane, which makes 16 beams in total, and the separation between two adjacent beams in the same layer is about 2.3 mm, and the separation between the adjacent beams in the up and down layers is about 2.0 mm. In the current setup, the main obstacle to increase N is the geometrical size of the optical

devices [see detailed discussion in the supplementary materials of (*32*)]. The scalability can be improved by putting the loop into a cavity with a low-loss polarization–independent optical switch (*49*).

Implementation of the measurement

The optimal measurement is the projective measurement on the common eigenvectors of three commuting observables, $\sigma_3\sigma_2$, $\sigma_1\sigma_3$, and $\sigma_2\sigma_1$, which can be realized by the complete Bell measurement with a local operation, $e^{i\frac{\pi}{3\sqrt{3}}(\sigma_x+\sigma_y+\sigma_z)}$, acting on the polarization qubit. This is because the Bell states are the common eigenvectors of $\sigma_3\sigma_3$, $\sigma_2\sigma_2$, and $\sigma_1\sigma_1$, which can be transferred to the optimal observables via the local operation (see the Supplementary Materials for details). Such measurement can be realized deterministically without any postselection. The quality of the experimentally realized Bell measurements is quantified by the interference visibility when the input states are taken as the Bell states. With N up to 8, the interference visibility is as high as 0.998.

Estimation algorithm and error analysis

We use the maximum likelihood to estimate the three parameters. To experimentally obtain the SD of the estimation, we repeat the process K times and obtain K estimations. The SD for the estimation of each parameter, $\delta\hat{x}$, is then obtained from the distribution of the K realizations. The error for this experimentally obtained $\delta\hat{x}$, which we denote as $\Delta(\delta\hat{x})$, is well approximated by $\Delta(\delta\hat{x}) = \frac{\delta\hat{x}}{\sqrt{2(K-1)}}$ (*50*). The error bar in Figs. 4 and 5 are drawn according to this $\Delta(\delta\hat{x})$ obtained with $K = 1000$ and 30, respectively.

SUPPLEMENTARY MATERIALS

Supplementary material for this article is available at http://advances.sciencemag.org/cgi/content/full/7/1/eabd2986/DC1

REFERENCES AND NOTES

1. C. W. Helstrom, *Quantum Detection and Estimation Theory* (Academic Press, 1976).
2. A. S. Holevo, *Probabilistic and Statistical Aspects of Quantum Theory* (North-Holland, 1982).
3. S. L. Braunstein, C. M. Caves, G. J. Milburn, Generalized uncertainty relations: Theory, examples, and Lorentz invariance. *Ann. Phys.* **247**, 135–173 (1996).
4. V. Giovannetti, S. Lloyd, L. Maccone, Quantum-enhanced measurements: Beating the standard quantum limit. *Science* **306**, 1330–1336 (2004).
5. V. Giovannetti, S. Lloyd, L. Maccone, Quantum metrology. *Phys. Rev. Lett.* **96**, 010401 (2006).
6. T. Nagata, R. Okamoto, J. L. O'Brien, K. Sasaki, S. Takeuchi, Beating the standard quantum limit with four-entangled photons. *Science* **316**, 726–729 (2007).
7. B. L. Higgins, D. W. Berry, S. D. Bartlett, H. M. Wiseman, G. J. Pryde, Entanglement-free Heisenberg-limited phase estimation. *Nature* **450**, 393–396 (2007).
8. G. Y. Xiang, B. L. Higgins, D. W. Berry, H. M. Wiseman, G. J. Pryde, Entanglement-enhanced measurement of a completely unknown optical phase. *Nat. Photonics* **5**, 43–47 (2011).
9. S. Slussarenko, M. M. Weston, H. M. Chrzanowski, L. K. Shalm, V. B. Verma, S. W. Nam, G. J. Pryde, Unconditional violation of the shot-noise limit in photonic quantum metrology. *Nat. Photonics* **11**, 700–703 (2017).
10. S. Daryanoosh, S. Slussarenko, D. W. Berry, H. M. Wiseman, G. J. Pryde, Experimental optical phase measurement approaching the exact heisenberg limit. *Nat. Commun.* **9**, 4606 (2018).
11. H. Yuan, C.-H. F. Fung, Quantum parameter estimation with general dynamics. *NPJ Quantum Inf.* **3**, 14 (2017).
12. W. Heisenberg, Über den anschaulichen inhalt der quantentheoretischen kinematik und mechanik. *Z. Phys.* **43**, 172–198 (1927).
13. J. Kahn, Fast rate estimation of a unitary operation in SU(*d*). *Phys. Rev. A* **75**, 022326 (2007).
14. H. Imai, A. Fujiwara, Geometry of optimal estimation scheme for *SU* (*D*) channels. *J. Phys. A Math. Theor.* **40**, 4391–4400 (2007).
15. P. C. Humphreys, M. Barbieri, A. Datta, I. A. Walmsley, Quantum enhanced multiple phase estimation. *Phys. Rev. Lett.* **111**, 070403 (2013).
16. T. Baumgratz, A. Datta, Quantum enhanced estimation of a multidimensional field. *Phys. Rev. Lett.* **116**, 030801 (2016).
17. M. Szczykulska, T. Baumgratz, A. Datta, Multi-parameter quantum metrology. *Adv. Phys. X* **1**, 621–639 (2016).
18. Z. Hou, Z. Zhang, G.-Y. Xiang, C.-F. Li, G.-C. Guo, H. Chen, L. Liu, H. Yuan, Minimal tradeoff and ultimate precision limit of multiparameter quantum magnetometry under the parallel scheme. *Phys. Rev. Lett.* **125**, 020501 (2020).
19. H. Yuan, Sequential feedback scheme outperforms the parallel scheme for hamiltonian parameter estimation. *Phys. Rev. Lett.* **117**, 160801 (2016).
20. Y. Chen, H. Yuan, Maximal quantum fisher information matrix. *New J. Phys.* **19**, 063023 (2017).
21. S. Ragy, M. Jarzyna, R. Demkowicz-Dobrzański, Compatibility in multiparameter quantum metrology. *Phys. Rev. A* **94**, 052108 (2016).
22. M. D. Vidrighin, G. Donati, M. G. Genoni, X.-M. Jin, W. S. Kolthammer, M. S. Kim, A. Datta, M. Barbieri, I. A. Walmsley, Joint estimation of phase and phase diffusion for quantum metrology. *Nat. Commun.* **5**, 3532 (2014).
23. E. Bagan, M. A. Ballester, R. D. Gill, R. Muñoz Tapia, O. Romero-Isart, Separable measurement estimation of density matrices and its fidelity gap with collective protocols. *Phys. Rev. Lett.* **97**, 130501 (2006).
24. N. Li, C. Ferrie, J. A. Gross, A. Kalev, C. M. Caves, Fisher-symmetric informationally complete measurements for pure states. *Phys. Rev. Lett.* **116**, 180402 (2016).
25. H. Zhu, M. Hayashi, Universally fisher-symmetric informationally complete measurements. *Phys. Rev. Lett.* **120**, 030404 (2018).
26. X.-Q. Zhou, H. Cable, R. Whittaker, P. Shadbolt, J. L. O'Brien, J. C. Matthews, Quantum-enhanced tomography of unitary processes. *Optica* **2**, 510–516 (2015).
27. M. A. Ciampini, N. Spagnolo, C. Vitelli, L. Pezzè, A. Smerzi, F. Sciarrino, Quantum-enhanced multiparameter estimation in multiarm interferometers. *Sci. Rep.* **6**, 28881 (2016).
28. E. Roccia, I. Gianani, L. Mancino, M. Sbroscia, F. Somma, M. G. Genoni, M. Barbieri, Entangling measurements for multiparameter estimation with two qubits. *Quantum Sci. Technol.* **3**, 01LT01 (2018).
29. Z. Hou, J.-F. Tang, J. Shang, H. Zhu, J. Li, Y. Yuan, K.-D. Wu, G.-Y. Xiang, C.-F. Li, G.-C. Guo, Deterministic realization of collective measurements via photonic quantum walks. *Nat. Commun.* **9**, 1414 (2018).
30. E. Polino, M. Riva, M. Valeri, R. Silvestri, G. Corrielli, A. Crespi, N. Spagnolo, R. Osellame, F. Sciarrino, Experimental multiphase estimation on a chip. *Optica* **6**, 288–295 (2019).
31. J.-F. Tang, Z. Hou, J. Shang, H. Zhu, G.-Y. Xiang, C.-F. Li, G.-C. Guo, Experimental optimal orienteering via parallel and antiparallel spins. *Phys. Rev. Lett.* **124**, 060502 (2020).
32. Z. Hou, R.-J. Wang, J.-F. Tang, H. Yuan, G.-Y. Xiang, C.-F. Li, G.-C. Guo, Control-enhanced sequential scheme for general quantum parameter estimation at the heisenberg limit. *Phys. Rev. Lett.* **123**, 040501 (2019).
33. M. A. Taylor, J. Janousek, V. Daria, J. Knittel, B. Hage, H.-A. Bachor, W. P. Bowen, Biological measurement beyond the quantum limit. *Nat. Photonics* **7**, 229–233 (2013).
34. Y. Israel, S. Rosen, Y. Silberberg, Supersensitive polarization microscopy using noon states of light. *Phys. Rev. Lett.* **112**, 103604 (2014).
35. Z. Hou, H. Zhu, G.-Y. Xiang, C.-F. Li, G.-C. Guo, Achieving quantum precision limit in adaptive qubit state tomography. *npj Quantum Inf.* **2**, 16001 (2016).
36. P. M. Birchall, E. J. Allen, T. M. Stace, J. L. O'Brien, J. C. F. Matthews, H. Cable, Quantum optical metrology of correlated phase and loss. *Phys. Rev. Lett.* **124**, 140501 (2020).
37. S. D. Bartlett, T. Rudolph, R. W. Spekkens, Reference frames, superselection rules, and quantum information. *Rev. Mod. Phys.* **79**, 555 (2007).
38. C. L. Degen, F. Reinhard, P. Cappellaro, Quantum sensing. *Rev. Mod. Phys.* **89**, 035002 (2017).
39. D. Brody, E.-M. Graefe, Information geometry of complex hamiltonians and exceptional points. *Entropy* **15**, 3361–3378 (2013).
40. S. Pang, T. A. Brun, Quantum metrology for a general hamiltonian parameter. *Phys. Rev. A* **90**, 022117 (2014).
41. D. J. Griffiths, D. F. Schroeter, *Introduction to Quantum Mechanics* (Cambridge Univ. Press, 2018).
42. H. Yuan, C.-H. F. Fung, Fidelity and fisher information on quantum channels. *New J. Phys.* **19**, 113039 (2017).
43. T. Juffmann, B. B. Klopfer, T. L. Frankort, P. Haslinger, M. A. Kasevich, Multi-pass microscopy. *Nat. Commun.* **7**, 12858 (2016).
44. P. M. Carlton, J. Boulanger, C. Kervrann, J.-B. Sibarita, J. Salamero, S. Gordon-Messer, D. Bressan, J. E. Haber, S. Haase, L. Shao, L. Winoto, A. Matsuda, P. Kner, S. Uzawa, M. Gustafsson, Z. Kam, D. A. Agard, J. W. Sedat, Fast live simultaneous multiwavelength four-dimensional optical microscopy. *Proc. Natl. Acad. Sci. U.S.A.* **107**, 16016–16022 (2010).
45. M. A. Taylor, W. P. Bowen, Quantum metrology and its application in biology. *Phys. Rep.* **615**, 1–59 (2016).
46. V. Cimini, M. Mellini, G. Rampioni, M. Sbroscia, L. Leoni, M. Barbieri, I. Gianani, Adaptive tracking of enzymatic reactions with quantum light. *Opt. Express* **27**, 35245–35256 (2019).

47. The LIGO Scientific Collaboration, A gravitational wave observatory operating beyond the quantum shot-noise limit. *Nat. Phys.* **7**, 962–965 (2011).
48. P. G. Kwiat, E. Waks, A. G. White, I. Appelbaum, P. H. Eberhard, Ultrabright source of polarization-entangled photons. *Phys. Rev. A* **60**, R773 (1999).
49. J.-F. Tang, Z. Hou, Q.-F. Xu, G.-Y. Xiang, C.-F. Li, G.-C. Guo, Polarization-independent coherent spatial-temporal interface with low loss. *Phys. Rev. Appl.* **12**, 064058 (2019).
50. S. Ahn, J. A. Fessler, *Standard Errors of Mean*, *Variance*, *and Standard Deviation Estimators* (EECS Department, The University of Michigan, 2003), pp. 1–2.

Acknowledgments
Funding: The work at USTC is supported by the National Natural Science Foundation of China (grant nos. 11574291, 11774334, 61905234, and 11974335), the National Key Research and Development Program of China (nos. 2017YFA0304100 and 2018YFA0306400), the Key Research Program of Frontier Sciences, CAS (no. QYZDY-SSW-SLH003), the Fundamental Research Funds for the Central Universities (no. WK2470000026), and China Postdoctoral Science Foundation (grant nos. 2016 M602012 and 2018 T110618). The work at CUHK is supported by RGC of Hong Kong (GRF no. 14308019). **Author contributions:** G.-Y.X. and H.Y. proposed the project. G.-Y.X. conceived and supervised the experiment. H.Y., Z.H., and H.C. developed the theoretical framework. Z.H., J.-F.T. and G.-Y.X. designed the experiment and the measurement apparatus. J.-F.T. constructed the setup, performed the experiment, and collected the data with assistance from Z.H. and G.-Y.X. J.-F.T., Z.H., H.Y., and G.-Y.X. performed numerical simulations and analyzed the experimental data with assistance from C.-F.L. and G.-C.G. Z.H., H.Y., G.-Y.X., H.C., and J.-F.T. developed the interpretation from uncertainty principle and wrote the manuscript. **Competing interests:** The authors declare that they have no competing interests. **Data and materials availability:** All data needed to evaluate the conclusions in the paper are present in the paper and/or the Supplementary Materials. Additional data related to this paper may be requested from the authors.

Submitted 12 June 2020
Accepted 6 November 2020
Published 1 January 2021
10.1126/sciadv.abd2986

Citation: Z. Hou, J.-F. Tang, H. Chen, H. Yuan, G.-Y. Xiang, C.-F. Li, G.-C. Guo, Zero–trade-off multiparameter quantum estimation via simultaneously saturating multiple Heisenberg uncertainty relations. *Sci. Adv.* **7**, eabd2986 (2021).